Photon-hadron and photon-photon collisions in CMS

Patricia Rebello Teles on behalf of the CMS Collaboration
Centro Brasileiro de Pesquisas Fisicas - CBPF
Rio de Janeiro - RJ, 22290-180, Brazil

E-mail: patricia.rebello.teles@cern.ch

Abstract. In this plenary talk given at PHOTON 2015 conference, the analyses performed in CMS experiment at the LHC on the photoproduction of coherent J/Ψ, accompanied by forward neutron emission, in ultra-peripheral lead-lead collisions at $\sqrt{s}_{NN} = 2.76$ TeV based on data sample collected in 2011, and the evidence for exclusive two-photon production of gauge boson $W^{\pm}$ pairs using the full $\sqrt{s} = 8$ TeV dataset collected during 2012 were presented.

1. The CMS detector

A detailed description of the CMS detector can be found in Ref. [1]. According Figure 1, in the central part of the apparatus are located the Electromagnetic and Hadronic calorimeters (ECAL and HCAL, respectively). The forward component of the hadronic calorimeter, the HF (Hadronic Forward), covers the $2.9 < |\eta| < 5.2$ region. In Figure 2, the very forward angles are covered at one end of CMS (the $6.6 < |\eta| < 5.2$ region) by the CASTOR calorimeter. In addition, the Beam Scintillator Counters (BSC) and the Zero Degree Calorimeters (ZDC) are sensitive to neutrons and photons with $|\eta| > 8.3$. The calorimeters coverage helps to ensure exclusivity measurements as well.

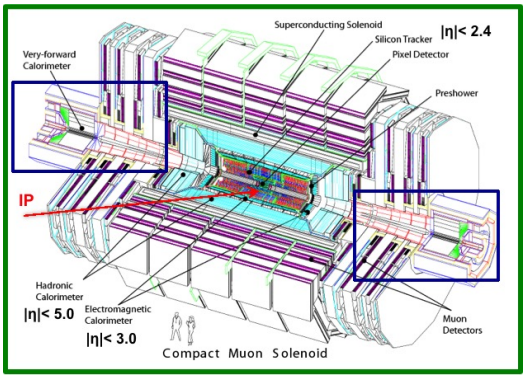

Figure 1. CMS detector general view. The blue boxes show the forward region detailed in Figure 2.

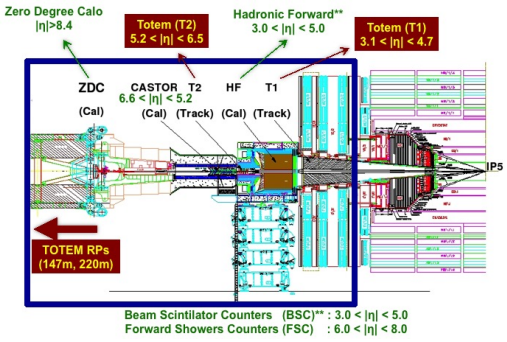

Figure 2. The forward region of the CMS detector in details.

2. Photon-Hadron at CMS: Photoproduction of the coherent J/ψ accompanied by the forward neutron emission in ultra-peripheral lead-lead collisions

Photon-nucleus and photon-photon are abundantly produced at LHC. In particular, as shown in Figure 3, the ultra-peripheral collision (UPC) of heavy ions involves electromagnetic interactions at impact parameters b larger than the sum of the radii of the colliding nuclei R [2].

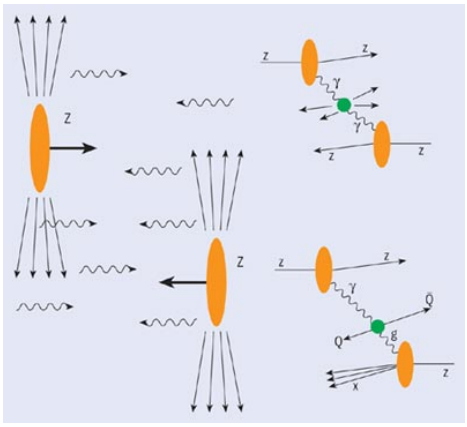

Figure 3. Ultra-peripheral collisions of heavy ions.

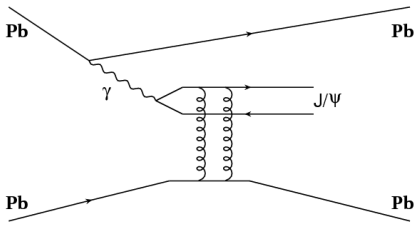

Figure 4. Coherent J/Ψ photoproduction in ultra-peripheral collisions of lead-lead.

In Figure 4 is shown the Feynman diagram of the coherent J/Ψ photoproduction in UPC of lead-lead. The results presented here were obtained by the CMS experiment, in the rapidity region $1.8 < |y| < 2.3$, with LHC running at center-of-mass energy $\sqrt{s}_{NN} = 2.76$ TeV.

The J/Ψ candidates are reconstructed through the dimuon decay channel while associated neutrons are detected in the Zero Degree Calorimeters (ZDC) shown in Figure 2). In addition, photon-photon collisions are studied using dimuon events in the invariant mass interval between 4 and 8 GeV/c^2 .

The four nuclear breakup modes discussed here are:

(i) X_n0_n: the dominant mode where one of the ZDC detects at least one neutron n while the other ZDC has no signal;

(ii) X_nX_n: both ZDC detect at least one neutron n;

(iii) 1_n0_n: one of the ZDC detects exactly one neutron n while the other has no signal;

(iv) 1_n1_n: both ZDC detect exactly one neutron n;

Only events with opposite-sign dimuons, produced in the X_n0_n breakup mode, having a dimuon $p_T < 1.0$ GeV/c and an invariant mass between 2.6 and 3.5 GeV/c^2 are considered. Figure 5 shows the dimuon invariant mass and the transverse momentum distributions from opposite-sign muon pairs for the X_n0_n breakup mode after all selection cuts.

The total systematic and statistical uncertainties in the J/Ψ coherent cross section are estimated to be 11% and 12%, respectively. Each contribution is listed in Table 1. Acceptance and efficiency correction factor, $(A \times \epsilon)_{J/\Psi}$, including the efficiency for the other selection cuts, corresponds to 5.9%.

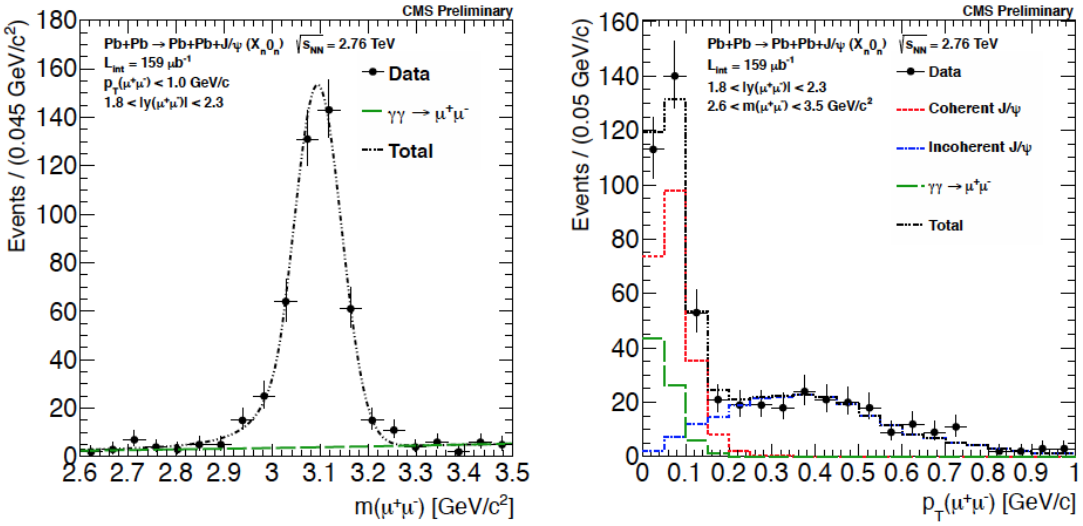

Figure 5. Dimuon invariant mass (left) and transverse momentum (right) distributions from opposite-sign muon pairs with $p_T < 1.0$ GeV/c and $2.6 < m(\mu^+\mu) < 3.5$ GeV/c^2 for the X_n0_n breakup mode after all selection cuts. Only statistical uncertainties are shown. The green histogram represents the $\gamma\gamma$ component and the black histogram the sum of the $\gamma\gamma$, incoherent J/Ψ and coherent J/Ψ components, respectively.

Table 1. Summary of systematic uncertainties.

	Uncertainty
Neutron tagging	6%
HF energy cut	1%
signal extraction	5%
MC input	1%
ZDC efficiency estimation	3%
Tracking reconstruction	4%
Luminosity determination	5%
Branching ration	1%

Results

For coherent J/Ψ production with $p_T < 0.15$ GeV/c, the ratios from the data and theory between different breakup modes normalized to the X_n0_n mode for both STARLIGHT and GSZ calculations in Table 2 show a good description. This is the first measurement of breakup ratios for J/Ψ production in ultra-peripheral collisions.

The resulting cross section for the X_n0_n mode is

$$\frac{d\sigma^{coh}_{X_n0_n}}{dy}(J/\Psi) = \frac{N^{J/\Psi}_{coh}}{BR(J/\Psi \to \mu^+\mu^-) \cdot \mathcal{L}_{int} \cdot \Delta y \cdot (A \times \epsilon)^{J/\Psi}} = 0.37 \pm 0.04(\text{stat}) \pm 0.04(\text{syst}) \text{ mb},$$

Table 2. Ratios from the data and theory between the modes X_nX_n, 1_n0_n, 1_n1_n and the mode X_n0_n. Only statistical errors.

J/Ψ with $p_T < 0.15$ GeV/c	X_nX_n/X_n0_n	$1_n0_n/X_n0_n$	$1_n1_n/X_n0_n$
Data	0.36±0.04	0.26±0.03	0.03±0.01
STARLIGHT	0.37	N/A	0.02
GSZ	0.32	0.30	0.02

where $BR(J/\Psi \to \mu^+\mu^-) = 5.93 \pm 0.06$ (syst)% is the branching ration of J/Ψ to dimuons, $N_{coh}^{J/\Psi} = 207 \pm 18$ is the coherent yield of J/Ψ with $p_T < 0.15$ GeV/c, $\mathcal{L}_{int} = 159\mu b^{-1}$ is the integrated luminosity, $\Delta y = 1$ is the rapidity bin width and $(A \times \epsilon)^{J/\Psi} = 5.9 \pm 0.5$ (stat)% is the combined correction factor.

Figure 6 shows that data favor calculations including nuclear gluon shadowing via the GSZ-LTA model [5], suggesting a significant reduction in the density of soft gluons within the nucleus that means a direct evidence of nuclear gluon shadowing at small-x values at LHC.

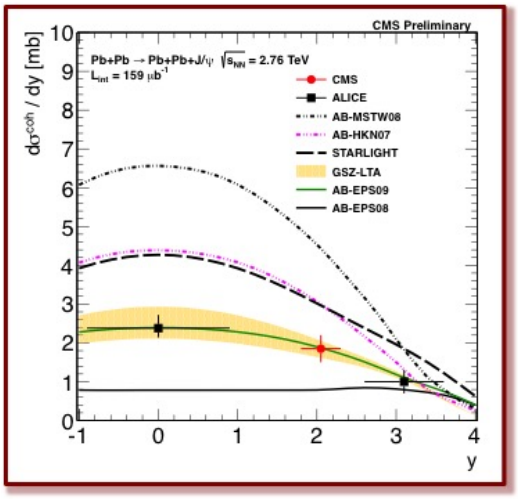

Figure 6. Differential cross section versus rapidity for coherent J/Ψ production in the X_n0_n breakup mode in UPC of PbPb at $\sqrt{s}_{NN} = 2.76$ TeV. The yellow band shows the theoretical uncertainty in the GSZ-LTA calculations. The horizontal bars represent the range of the measurement in rapidity $|y|$.

3. Photon-Photon at CMS: Evidence for exclusive $\gamma\gamma \to W^+W^-$ production and constraints on anomalous quartic gauge couplings

The LHC studies of high-energy photon-photon interactions, thanks to its high energy and large integrated luminosity, occur at leading order via the diagrams shown in Figure 7.

Such studies are well suited to search for physics beyond the Standard Model (SM) through deviations that may be quantified by genuine anomalous quartic gauge couplings, according to the following effective operators of dimension-6 and dimension-8 [6]:

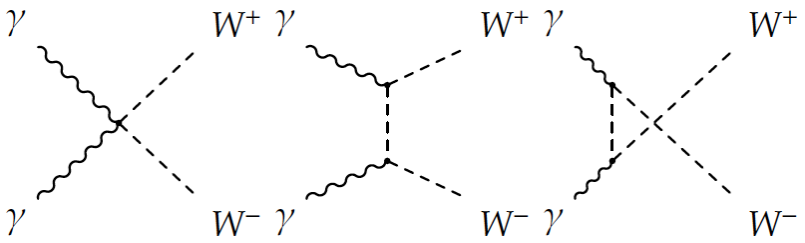

Figure 7. Diagrams contributing to the $\gamma\gamma \to W^+W^-$ process at leading order in the SM.

$$
\begin{aligned}
L_6^0 &= \frac{e^2}{8}\frac{a_0^W}{\Lambda^2} F_{\mu\nu}F^{\mu\nu}W^{+\alpha}W^-_{\alpha} \\
L_6^C &= -\frac{e^2}{16}\frac{a_C^W}{\Lambda^2} F_{\mu\alpha}F^{\mu\beta}(W^{+\alpha}W^-_{\beta} + W^{-\alpha}W^+_{\beta}) \\
L_8^{M,0} &= \mathrm{Tr}[\hat{W}_{\mu\nu}\hat{W}^{\mu\nu}] \times [(D_\beta\Phi)^\dagger D^\beta\Phi] \\
L_8^{M,1} &= \mathrm{Tr}[\hat{W}_{\mu\nu}\hat{W}^{\nu\beta}] \times [(D_\beta\Phi)^\dagger D^\alpha\Phi] \\
L_8^{M,2} &= [B_{\mu\nu}B^{\mu\nu}] \times [(D_\beta\Phi)^\dagger D^\beta\Phi] \\
L_8^{M,3} &= [B_{\mu\nu}B^{\nu\beta}] \times [(D_\beta\Phi)^\dagger D^\mu\Phi]
\end{aligned}
$$

In dimension-8 formalism there are fourteen operators contributing to γ couplings, which in general will also generate $WWZ\gamma$ vertex. By including an additional constraint that the $WWZ\gamma$ vertex should vanish, a direct relationship between the dimension-8 couplings and the dimension-6 couplings can be recovered as

$$
\begin{aligned}
\frac{a_0^W}{\Lambda^2} &= -\frac{4M_W^2}{g^2}\frac{f_{M,0}}{\Lambda^4} - \frac{8M_W^2}{g'^2\frac{f_{M,2}}{\Lambda^4}} \\
\frac{a_C^W}{\Lambda^2} &= \frac{4M_W^2}{g^2}\frac{f_{M,1}}{\Lambda^4} + \frac{8M_W^2}{g'^2\frac{f_{M,3}}{\Lambda^4}}
\end{aligned}
$$

where M_W is the mass of the W boson, $g = e/\sin(\theta_W)$ and $g' = e/\cos(\theta_W)$.

To prevent the increasing of the $\gamma\gamma \to W^+W^-$ cross section with the photon-photon center-of-mass energy $W_{\gamma\gamma}$, and consequently the violation of unitariry at scales below those reached in 8 TeV p-p collisions, on both dimension-6 and dimension-8 scenarios one can consider a dipole form factor with a cutoff scale $\Lambda_{cutoff} = 500$ GeV (unitariry violating limits with $\Lambda_{cutoff} \to \infty$ is equivalent to no form factor):

$$
a_{0,C}^W(W_{\gamma\gamma}^2) = \frac{a_{0,C}^W}{(1 + \frac{W_{\gamma\gamma}^2}{\Lambda_{cutoff}^2})}.
$$

In this talk we present the update of the 7 TeV CMS publication concerning the $\gamma\gamma \to W^+W^-$ channel [7], largely following its same strategy. It uses the full dataset collected during 2012 consisting of 19.7 fb^{-1} of proton-proton collisions at center-of-mass energy of $\sqrt{s} = 8$ TeV

Table 3. Number of expected signal and background events in MC simulation. Uncertainties are statistical only.

Selection step	Excl. $\gamma\gamma \to WW$	Total Background	WW+jets	$\gamma\gamma \to \tau\tau$	DY $\to \tau\tau$	Diffractive WW	Other Backgrounds
Trigger and preselection	26.9±0.2	12560±230	1057.5±8.1	18.1±0.8	7000±75	206.2±3.0	4280±210
$m(\mu^{\pm}e^{\mp}) > 20$ GeV	26.6±0.2	12370±220	1035.5±8.0	18.1±0.8	6974±75	202.2±3.0	4140±210
Electron and Muon ID	22.5±0.2	6458±93	1027.9±8.0	12.6±0.7	4172±58	197.2±2.9	1048±72
$\mu^{\pm}e^{\mp}$ vertex with 0 extra tracks	6.7±0.2	14.9±2.5	2.8±0.4	4.3±0.5	6.5±2.3	0.3±0.1	1.1±0.6
$p_T(\mu^{\pm}e^{\mp}) > 30$ GeV	5.3±0.1	3.5±0.5	2.0±0.4	0.9±0.2	0	0.1±0.1	0.5±0.2

Table 4. Summary of systematic uncertainties.

	Uncertainty
Proton dissociation factor	10.5%
Efficiency Correction for 0 extra tracks	5.0%
Trigger and lepton ID	2.4%
Luminosity	2.6%
Total	12.1%

combined with that from the analysis carried out in 2011 using 5.05 fb^{-1} at $\sqrt{s} = 7$ TeV. During the 8 (7) TeV data-taking period of the LHC the mean number of overlapping interactions per bunch crossing was 21 (9).

The signal region is defined by the presence of opposite-sign electron-muon pair $e^{\pm}\mu^{\mp}$, originating from a common primary vertex that has no additional tracks associated with it, with $p_T(e^{\pm}\mu^{\mp}) > 30$ GeV.

In order to select a high-purity sample of elastic $pp \to p\ l^{\pm}\ l^{\mp}\ p$ events and to study the efficiency of the zero extra tracks requirement, we apply tight selection criteria to the kinematics of the lepton pair [6]:

- small acoplanarity requirement: $|1 - \Delta\phi(l^{\pm}l^{\mp})/\pi| < 0.01$;
- invariant mass outside M_Z window: 70 GeV $< m(l^{\pm}l^{\mp}) <$ 106 GeV;
- zero extra tracks at dilepton vertex to remove most of the inclusive $W^{\pm}W^{\mp}$ background;
- $p_T(e^{\pm}\mu^{\mp}) > 30$ GeV for supress $\gamma\gamma \to \tau\tau$.

The number of expected signal and background events for Monte Carlo simulation in each stage of the selection with an opposite sign muon and electron associated to the same vertex, each with $p_T > 20$ GeV and $|\eta| < 2.4$, and less than 16 additional tracks at the vertex for an integrated luminosity of 19.7 fb^{-1} is shown in Table 3.

Systematic uncertainties, listed in Table 4, were considered according to the luminosity, the lepton trigger and selection efficiency, the efficiency of the zero extra tracks requirement, and the uncertainty in the proton dissociation contribution.

Results

As shown in Figure 8, in the signal region with 0 extra tracks and $p_T(e^{\pm}\mu^{\mp}) > 30$ GeV, 13 events are observed in the data that pass all the selection criteria over 3.5±0.5 (stat.) events expected for background and 5.3±0.1 (stat.) expected for the signal. Therefore the observed significance above the background-only hypothesis in the 8 TeV data, including systematic uncertainties, is 3.6 σ.

Interpreting the 8 TeV results as a W^+W^- production cross section multiplied by the branching ratio to the $e^{\pm}\mu^{\mp}$ final states, corrected for all experimental efficiencies and extrapolated to the full phase space, we have found the value

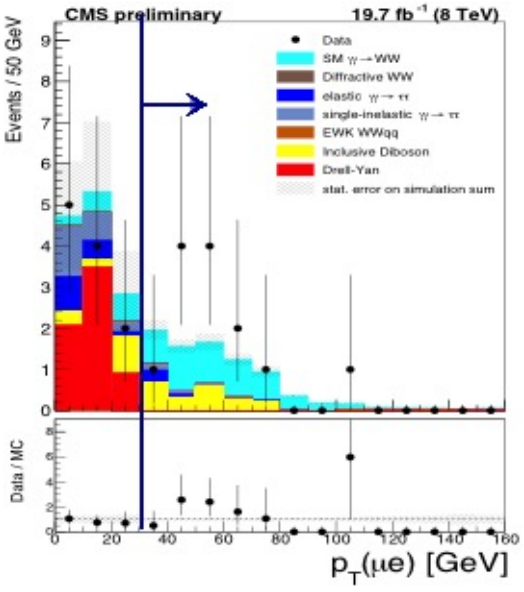

Figure 8. Transverse momentum distribution (on the left) for the signal region with 0 extra tracks and $p_T(e^{\pm}\mu^{\mp}) > 30$ GeVwhere 13 events can be observed in the data that pass all the selection criteria.

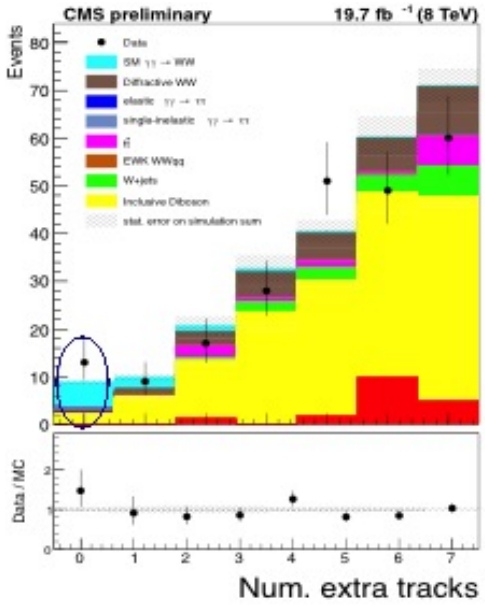

Figure 9. Number of extra tracks distribution showing the observed 13 events in the signal region with 0 extra tracks.

$$\sigma(pp \to p^{(*)}W^+W^-p^{(*)} \to p^{(*)}\mu^{\pm}e^{\mp}p^{(*)}) = 12.3^{+5.5}_{-4.4} \text{ fb}.$$

In Figure 10, muon-electron invariant mass, acoplanarity, and missing transverse energy distributions in the $\gamma\gamma \to W^+W^-$ signal region show a good agreement in shape with data (shown by points with error bars). The histograms indicate the expected SM signal and backgrounds.

Furthermore, the dilepton transverse momentum was used as a discriminating variable to extract limits on anomalous quartic gauge couplings (AQGC). Table 5 summarizes all of the limits on the dimension-6 and dimension-8 AQGC parameters obtained with 8 TeV CMS data. The limits are 7–16 times more stringent than search for $WW\gamma$ and $WZ\gamma$ production [8] and 3–7 times more stringent than the same-sign vector boson Scattering analysis [9].

A similar procedure was followed to derive two dimensional limits in the a_0^W/Λ^2, a_C^W/Λ^2 parameter space for the unitarized results with $\Lambda_{cutoff} = 500$GeV. The two dimensional 95% confidence regions obtained from $\gamma\gamma \to W^+W^-$ production at CMS are shown in Figure 11.

Acknowledgments

The author thanks Valery Telnov and the CMS collaboration for supporting. This work is partly supported by the Brazilian Science without Borders Program from Coordination for the Improvement of Higher Education Personnel (CAPES) grant BEX 11767-13-8.

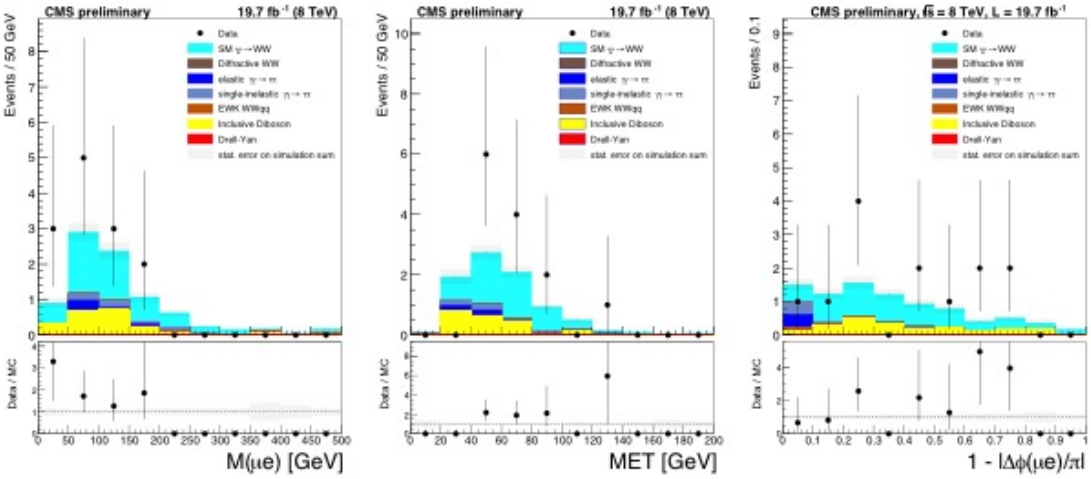

Figure 10. Muon-electron invariant mass (left), acoplanarity (center), and missing transverse energy (right) distributions in the $\gamma\gamma \to W^+W^-$ signal region.

Table 5. Summary of all 95% CL AQGC limits derived from the measured $p_T(e\mu)$ distributions in the $\gamma\gamma \to W^+W^-$ signal region production in CMS at 8 TeV.

Dimension-6 AQGC parameter	8 TeV ($\times 10^{-4}$GeV^{-2})
$a_0^W/\Lambda^2(\Lambda_{cutoff} = 500\text{GeV})$	$-1.1 < a_0^W/\Lambda^2 < 1.0$
$a_C^W/\Lambda^2(\Lambda_{cutoff} = 500\text{GeV})$	$-4.2 < a_C^W/\Lambda^2 < 3.4$
Dimension-8 AQGC parameter	8 TeV ($\times 10^{-10}$GeV^{-4})
$f_{M,0}/\Lambda^4(\Lambda_{cutoff} = 500\text{GeV})$	$-3.8 < f_{M,0}/\Lambda^4 < 4.2$
$f_{M,1}/\Lambda^4(\Lambda_{cutoff} = 500\text{GeV})$	$-16 < f_{M,1}/\Lambda^4 < 13$
$f_{M,2}/\Lambda^4(\Lambda_{cutoff} = 500\text{GeV})$	$-1.9 < f_{M,2}/\Lambda^4 < 2.1$
$f_{M,3}/\Lambda^4(\Lambda_{cutoff} = 500\text{GeV})$	$-8.0 < f_{M,3}/\Lambda^4 < 6.4$
Dimension-6 AQGC parameter	8 TeV ($\times 10^{-6}$GeV^{-2})
a_0^W/Λ^2(no form factor)	$-1.2 < a_0^W/\Lambda^2 < 1.2$
a_C^W/Λ^2(no form factor)	$-4.4 < a_C^W/\Lambda^2 < 4.4$
Dimension-8 AQGC parameter	8 TeV ($\times 10^{-12}$GeV^{-4})
$f_{M,0}/\Lambda^4$(no form factor)	$-4.6 < f_{M,0}/\Lambda^4 < 4.6$
$f_{M,1}/\Lambda^4$(no form factor)	$-17 < f_{M,1}/\Lambda^4 < 17$
$f_{M,2}/\Lambda^4$(no form factor)	$-2.3 < f_{M,2}/\Lambda^4 < 2.3$
$f_{M,3}/\Lambda^4$(no form factor)	$-8.3 < f_{M,3}/\Lambda^4 < 8.3$

References

[1] CMS Collaboration, JINST 03 (2008) S08004.
[2] CMS Collaboration, CMS PAS HIN-12-009
[3] M. Ryskin, Z. Phys. **C57** (1993).
[4] S.J. Brodsky et al., Phys. Rev. **D50** (1994).
[5] V. Guzey, M. Strikman, and M. Zhalov, , Eur.Phys.J. C74 (2014).
[6] CMS Collaboration, CMS PAS FSQ-13-008.
[7] CMS Collaboration, J. High Energy Phys. **07** (May, 2013)
[8] CMS Collaboration, Phys. Rev. D 90, 032008 (2014)
[9] CMS Collaboration, Phys. Rev. Lett. 114, 051801 (2015)

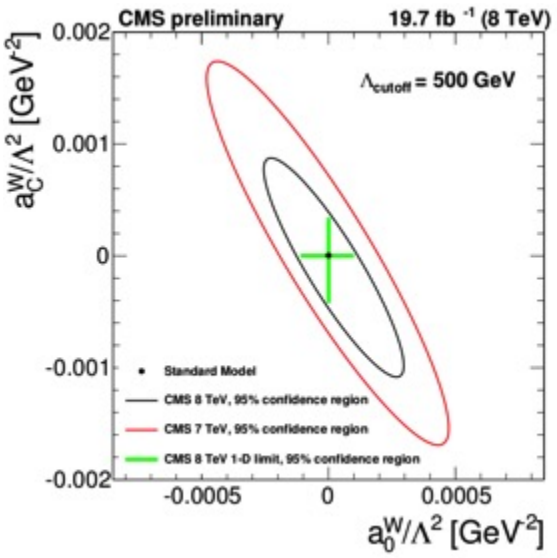

Figure 11. The two dimensional 95% CL regions obtained in the $\gamma\gamma \to W^+W^-$ signal region.